JOURNAL OF SYNCHROTRON RADIATION

Volume 25 (2018)

Supporting information for article:

Energy-dependent dead-time correction in digital pulse processors applied to silicon drift detector's X-ray spectra

Suelen F. Barros, Vito R. Vanin, Alexandre A. Malafronte, Nora L. Maidana and Marcos N. Martins

Journal of Synchrotron Radiation

ISSN 1600-5775

Energy-dependent dead-time correction in digital pulse processors applied to Silicon Drift Detector's x-ray spectra
Supplementary material

Suelen F. Barros,[a]* Vito R. Vanin,[a] Alexandre A. Malafronte,[a] Nora L. Maidana[a] and Marcos N. Martins[a]

[a]Instituto de Física, Universidade de São Paulo.

Rua do Matão, 1371, Cidade Universitária. CEP:05508-090 São Paulo, SP, Brazil. Correspondence e-mail: suelenb@if.usp.br

Here we give a detailed account of the experiment, describe an unsuccessful attempt to model the growth of peak wings with rate, provide some more application examples, and show the results obtained when correcting the spectra according the simplest model following Table 2 in the main text.

1. Experiment

1.1. Experimental arrangement

The photon source consisted in the x-ray spectra produced by electrons hitting a thin Au film. The target consisted in a layer of Au (47 μg/cm^2) deposited on a thin C backing (14 μg/cm^2) and was prepared by physical vapour deposition technique. A carbon fibre holder placed the target in the center of the irradiation chamber, tilted 30° with respect to a plane normal to the direction of the incident beam. To obtain the spectra with few counts near the energy threshold a 25-μm thick kapton film was placed in front of the detector beryllium window.

The total charge incident on the target, which is proportional to the true input count rate, was evaluated from the sum of the charges collected in the Faraday cup and in the irradiation chamber, both electrically insulated.

1.2. Experimental procedure

The target was irradiated with a beam of 18.5 keV electrons. Beam current was varied from 10 to 700 nA to take spectra with counting rates in the range $1 - 56$ kHz, where 1 kHz $= 10^3$ *recorded* counts per second of acquisition time; the maximum attainable count rates (or throughput) with the time constants employed were about 97 and 88 kHz for the experiments using or not the x-ray attenuator, respectively.

Measurements without attenuator were taken at counting rates of 1, 3, 4, 12, 19, 26, 42, and 56 kHz; and with attenuator, at rates of 1, 4, 9, 18, 28, and 42 kHz. Runs lasted between 300 and 3600 s, according to the counting rate, to warrant similar counting statistics in all spectra.

1.3. DPP aquisition system

1.3.1. Spectrometer operation. The DPP has a single Analog to Digital Converter (ADC), and two analyser channels that process numerically the ADC output with different parameters, which can be characterized by a small set of quantities, like the rise-time of the obtained function. We refer to these numeric functions as pulses, since this is the purpose they fulfil. We also loosely speak about the voltage of these functions, since there is a correspondence between their numeric values and the voltage of the detector output, that does not need quantification for the models presented here.

This DPP slow digitizing channel has a conversion time in the μs range. The fast channel digitizer conversion time is of the order of 0.1 μs, and it is used to detect pile-up and subsequently veto the slow channel conversion. Each channel has a lower-level discriminator, which must be set above noise and defines the spectrum energy threshold. In the slow channel, the discriminator avoids continuous triggering of the digitizer, and in the fast, prevents the pile-up rejection system from firing uninterruptedly.

In order to set the threshold associated with the slow discriminator we followed the supplier's instructions. With the electron beam turned off, a data acquisition was run during 1 min with Pile Up Rejection (PUR) turned off. The first channel without noise counts is suggested as the ideal discriminator setting (Amptek A), which corresponded to $\approx$ 220 eV. It was reported that the minimum setting above noise of the slow discriminator provides an estimate of one of the dead-time model parameters (Redus *et al.*, 2008).

The fast threshold was chosen after comparison of spectra taken with counting rates about 18 kHz for settings between 500 and 1500 eV in 200 eV steps. They were examined for dead-time and event suppression due to incorrect pile-up rejection. Since photons with energies below 1 keV do not go through the Be detector window, we ran the experiment with the slow threshold set at a few hundred eV above the adopted noise level. The final settings were 660 eV and 1100 eV for the slow and fast thresholds, respectively.

1.3.2. Pile-up in the DPP. With PUR turned on, the slow channel will register a pulse if its peak amplitude is above the slow-threshold setting and below full-scale, and the fast channel does not detect two pulses within the analysis time of the slow channel. However, the fast channel cannot avoid pile-up on its own input, hence when two pulses arrive within a time interval

shorter than the rise time of the fast channel, the slow channel will not be vetoed. Therefore, in the slow channel, the two signals will coalesce into a single pulse, which will be recorded in the spectrum channel that corresponds approximately to the sum of the amplitudes of both signals.

Thus, although the slow channel does not record events from pile-up associated to its (long) time constant, it will show events related to pile-up in the *fast* channel. Therefore, spectra obtained from the SDD at high rate (tens of kHz) must be corrected not only for losses from dead-time but also for distortions from pile-up, even when PUR is turned on during acquisition.

2. Pile-up events distribution function

The pile-up distribution function was modelled based on Vanin *et al.* (Vanin *et al.*, 2016), which is a simplified version of the equation given by Statham (Statham, 2006), using the same pulse resolution time for photons of all energies. It is more practical to develop the pile-up distribution as a function of the channel number, ℓ, instead of the photon energy, used in the formulas above. We adopt a photon energy calibration given by

$$E(\ell) = a + b\,\ell \tag{1}$$

with a and b fitted to experimental data. The number of events actually recorded by the SDD in the channel ℓ is

$$s(\ell) = \theta\, R_{\text{out}}\,(E(\ell), R_{\text{in}}) \tag{2}$$

where the constant θ is related to energy dispersion, beam current and acquisition time. However, we will not need θ anywhere else, since all other formulas in this work relate either counts per channel or rates — this equation is important conceptually, but not required in practice.

With the definitions above, the number of pile-up events $p(\ell)$ in channel ℓ can be well approximated by (Vanin *et al.*, 2016)

$$p(\ell) = \eta \sum_c s(\ell - c - k)\, s(c) \tag{3}$$

where k is the integer closest to (a/b), and η is a constant parameter, related to the fast digitizer time constants, eq. (11).

3. Quantifying peak shape distortions

There are multiple sources of noise in the detector's electronics that can pile-up with true pulses and change the spectrum shape, specially at high-rates (Radeka, 1972). We adopt Knoll (Knoll, 2010) definition for noise: "any undesired fluctuation that appears superimposed on a signal source". The most known type noise has a very broad frequency spectrum and widens the peaks corresponding to monochromatic radiation, but other sources can distort the peaks asymmetrically, generating wings (or shoulders) in one or both sides. In this section, we try to assess the contribution of all these phenomena to the acquired spectra, which is not included in eqs. (8) and (12); understanding what caused these other sources of noise is out of the scope of this work.

Noise events cannot be observed directly in the spectrum due to the DPP slow discriminator. However, pile-up with noise can be noticed when it occurs with pulses from a high intensity line (Nascimento *et al.*, 2011). Therefore, the noise contribution was evaluated from the comparison between the spectrum acquired at the lowest rate, $s_{\text{LR}}(\ell)$, with those obtained at high rates. Neglecting pile-up in the low rate spectrum, a pile-up-free estimate of the *compensated* spectrum acquired at rate $R_{\text{in},i}$ is

$$S_{i(\text{LR})}(\ell) = s_{\text{LR}}(\ell) \exp\left(R_{\text{in,LR}}\ \tau(\ell)\ \right)\ \frac{C_i}{C_{\text{LR}}} \tag{4}$$

which takes into account the charges collected in the acquisition runs at rates $R_{\text{in},i}$ and low-rate, respectively C_i and C_{LR}.

From the difference between the compensated spectrum acquired at rate $R_{\text{in},i}$ and this pile-up-free estimate of the same spectrum, the distortion caused in the spectrum due to pile-up with noise is estimated as

$$p_{n,i}(\ell) = S_i(\ell) - S_{i(\text{LR})}(\ell) \tag{5}$$

The distributions obtained with the formula above should have a null sum. However, we have found that this was not true at high counting rates in the ML spectra, where we observed differences amounting to about 0.6% of the number of counts in the spectrum taken at 56 kHz. One possible neglected effect that could account for this inconsistency is related to the DPP poorer resolution in the fast channel when compared to the slow channel. The selection of events near threshold may not be sufficiently sharp to isolate true low-energy events from noise as a consequence of a fuzzy fast threshold setting, making room for errors in the pile-up correction.

4. Additional Results

Figs. 1 and 2 show ML and L spectra, respectively, plotted as z-distributions corrected according to SMP_f. Figs. 3 and 4 corresponde to the same raw spectra, corrected for dead-time losses according to the EDP_g framework and replacing the reference spectrum $n_{\text{LR}}(E)$ by $\vec{\nu}$ in formula (25). Figs. 5 and 6 show the z-distributions for ML and L spectra corrected to 1.0% and 0.5% according to the models suggested in Table 2, adopting the reference spectrum $\nu(\ell)$ instead of n_{LR} in eq. (25).

References

Nascimento, E., Fernández-Varea, J. M., Vanin, V. R., Maidana, N. L. (2011). *AIP Conf. Proc.* ***1351****, 216-220.*

Radeka, V. (1972). *IEEE Trans. Nuc. Sci.* **19**, 412–428.

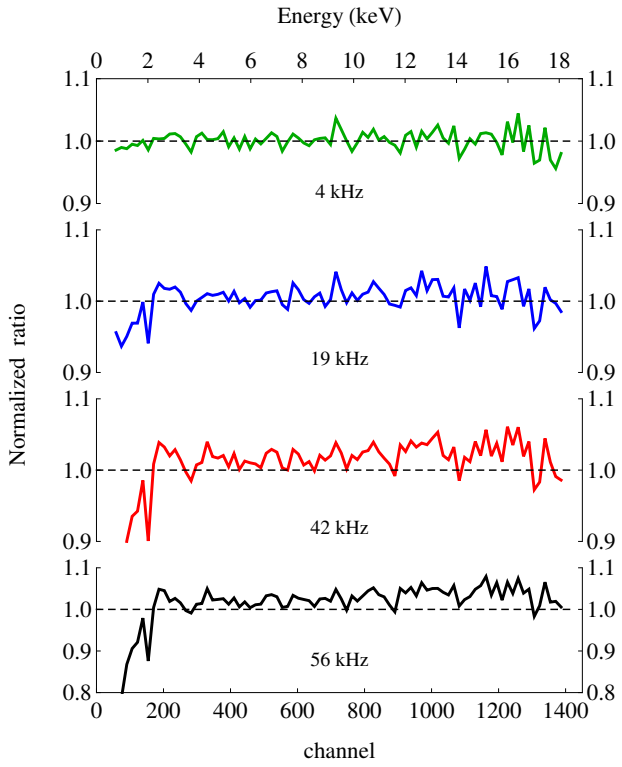

Figure 1
Ratio of some of the ML spectra, normalized by the incident charge and corrected for dead-time losses in the SMP$_f$ framework, to the spectrum acquired at the lowest rate, also normalized by the charge, eq.(25). The spectra were compressed, and each bin corresponds to 210 eV.

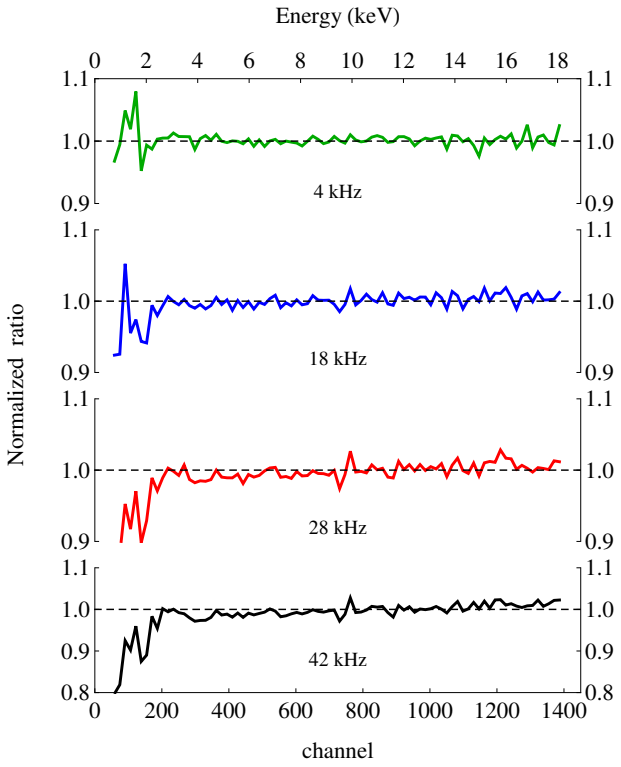

Figure 2
Same as fig. 1, but for L spectra.

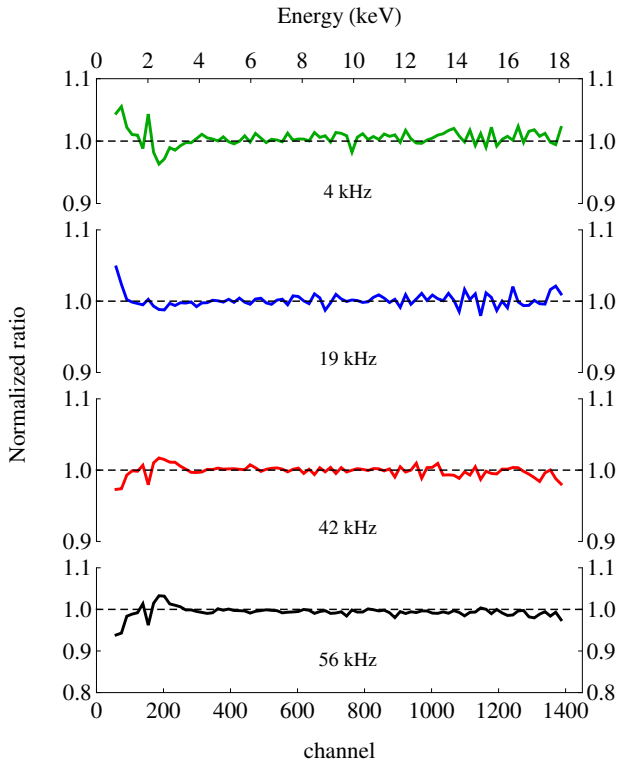

Figure 3
Ratio of ML spectra, normalized by the incident charge and corrected for dead-time losses in the EDP$_g$ framework, to the estimated reference spectrum $\nu(\ell)$. The spectra were compressed, and each bin corresponds to 210 eV.

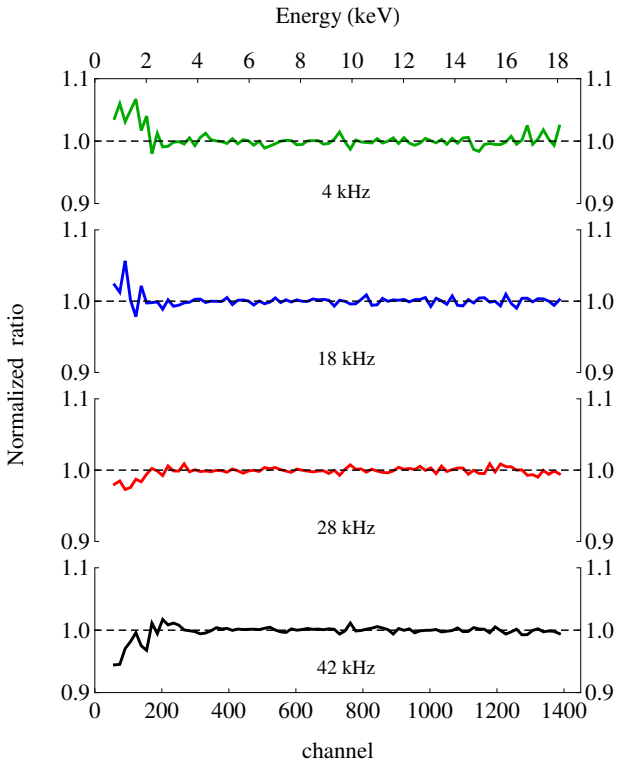

Figure 4
Same as fig. 3, but for L spectra.

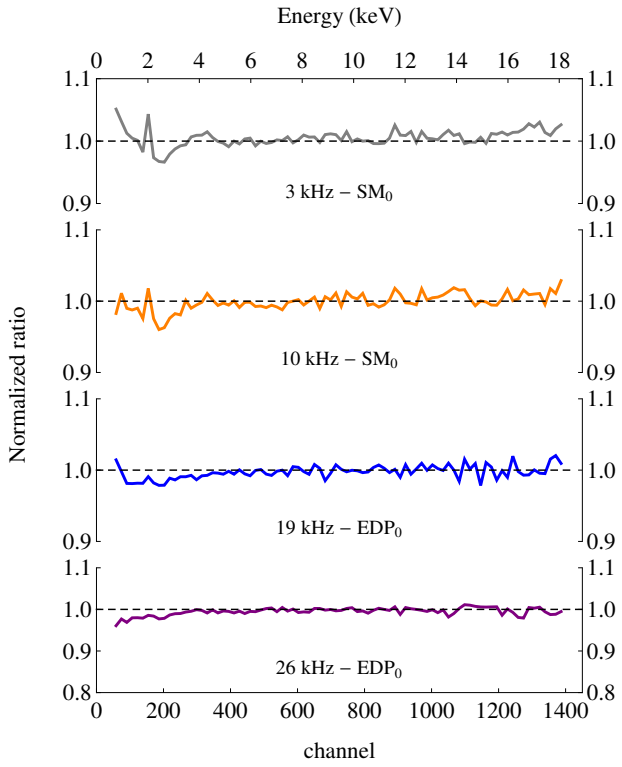

Figure 5
z-distributions, eq. (25), for ML spectra corrected to 1.0% according to the model suggested in Table 2, adopting the reference spectrum $\nu(\ell)$ determined from EDP_g model. The z-distributions for 42 kHz and 56 kHz can be found in Fig.3.

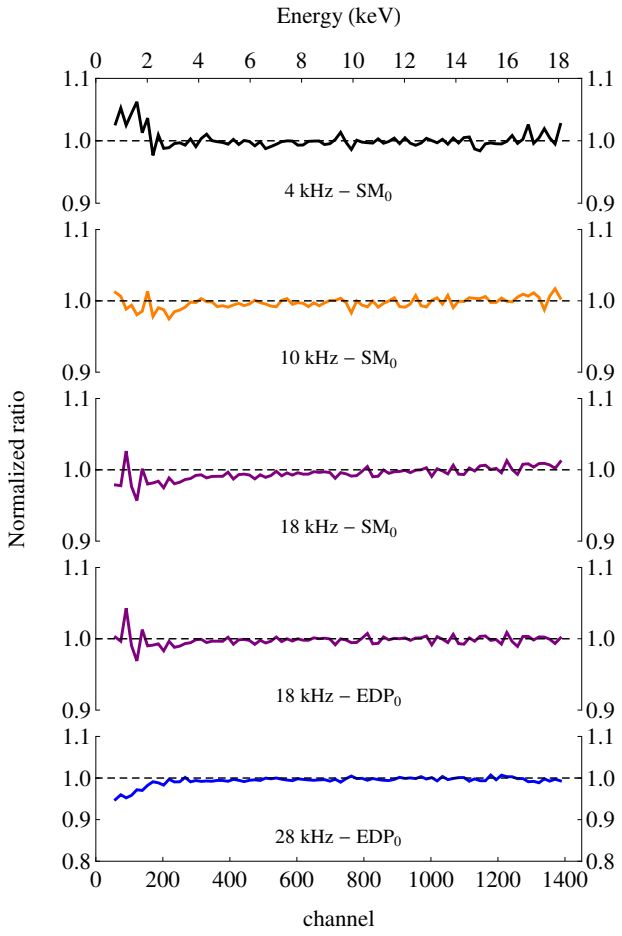

Figure 6
z-distributions, eq. (25), for L spectra corrected to 0.5% according to the model suggested in Table 2, adopting the reference spectrum $\nu(\ell)$ determined from EDP_g model. The z-distribution for 42 kHz can be found in Fig. 4.